Biochimica et Biophysica Acta 1848 (2015) 662–672

Contents lists available at ScienceDirect

Biochimica et Biophysica Acta

journal homepage: www.elsevier.com/locate/bbamem

# Atomically detailed lipid bilayer models for the interpretation of small angle neutron and X-ray scattering data

Joseph C. Fogarty [a], Mihir Arjunwadkar [b], Sagar A. Pandit [a,*], Jianjun Pan [a]

[a] Department of Physics, University of South Florida, Tampa, FL 33620, USA
[b] Centre for Modeling and Simulation, University of Pune, Pune 411007, India

ARTICLE INFO

*Article history:*
Received 25 July 2014
Received in revised form 11 October 2014
Accepted 29 October 2014
Available online 25 November 2014

*Keywords:*
Model membrane
SAXS
SANS
Simplex based optimization

ABSTRACT

We present a new atom density profile (ADP) model and a statistical approach for extracting structural characteristics of lipid bilayers from X-ray and neutron scattering data. Models for five lipids with varying head and tail chemical composition in the fluid phase, 1,2-dioleoyl-*sn*-glycero-3-phosphatidylcholine (DOPC), 1-palmitoyl-2-oleoyl-*sn*-glycero-3-phosphatidylcholine (POPC), 1,2-dipalmitoyl-*sn*-glycero-3-phosphatidylcholine (DPPC), 1-palmitoyl-2-oleoyl-*sn*-glycero-3-phosphatidylserine (POPS), and 1-palmitoyl-2-oleoyl-*sn*-glycero-3-phosphatidylglycerol (POPG), are optimized using a simplex based method to simultaneously reproduce both neutron and X-ray scattering data. Structural properties are determined using statistical analysis of multiple optimal model structures. The method and models presented make minimal assumptions regarding the atomic configuration, while taking into account the underlying physical properties of the system. The more general model and statistical approach yield data with well defined uncertainties, indicating the precision in determining density profiles, atomic locations, and bilayer structural characteristics. Resulting bilayer structures include regions exhibiting large conformational variation. Due to the increased detail in the model, the results demonstrate the possibility of a distinct hydration layer within the interfacial (backbone) region.



## 1. Introduction

Cell membranes participate in a host of vital biological functions. In order to understand the role of lipid membrane components in these functions, it is necessary to resolve membrane structures formed by single lipid species. This is achieved by studying model lipid bilayers with simple compositions. Thermal fluctuations of disordered lipid bilayers pose significant difficulty in determining atomic positions. Scattering techniques such as small angle X-ray (SAXS) and neutron (SANS) scattering have been traditionally used to explore structures of lipid bilayers. The utility of the SAXS and SANS methods is primarily due to their sensitivity to heterogeneous electron and neutron scattering length distributions. In particular, X-ray is scattered most strongly by electron dense moieties. Therefore, it is capable of localizing phospholipid phosphate groups. Due to the remarkable difference of neutron scattering length between hydrogen and other atoms including deuterium, neutron scattering is most suited for localization of the hydrogen deficient glycerol/carbonyl backbone. Since X-ray and neutron scattering profiles are dominated by different molecular features, more detailed information can be inferred by using their combination [1–9]. This hybrid approach (i.e. the simultaneous fitting of SAXS and SANS data from equivalent lipid bilayers) along with the scattering density profile (SDP) model has been applied to successfully extract structure of many commonly seen phosphatidylcholine (PC), phosphatidylglycerol (PG) and phosphatidylserine (PS) lipid bilayers [4–8]. The essence of the SDP model is to partition a lipid bilayer into several components each of whose volume probabilities and electron and neutron scattering length densities are described by one mathematical function (e.g., a Gaussian or an error function). The SDP model relies on proper grouping of lipid atoms, and the dimensionality that the model can handle is limited by the fitting procedure. Furthermore, many parameters need to be constrained to avoid instabilities in fitting. For example, in constraint-free analysis, the width of the error function describing hydrocarbon chains, and thus the hydrocarbon core thickness, tends to bloat. Finally, the SDP model relies on nonlinear least squares fitting methods, such as Levenberg–Marquardt. Levenberg–Marquardt can have slow convergence for problems with large residuals, which can result from noisy data [10]. Additionally, nonlinear least squares methods may be unsuitable for higher dimensions due to the growth of computational time with the size of the parameter space [11]. In the interest of dimensional reduction, the SDP model combines groups of atoms. The increased dimensionality for bilayer mixtures poses a non-trivial and difficult challenge for the SDP model. A more recent usage of the SDP model performed parameter optimization via a genetic algorithm which offers advantages (primarily the avoidance of local minima) over the more commonly used Levenberg–Marquardt [9].

* Corresponding author.
*E-mail address:* pandit@usf.edu (S.A. Pandit).

http://dx.doi.org/10.1016/j.bbamem.2014.10.041
0005-2736/

In general, scattering techniques provide reciprocal space structure, necessitating a transformation into real space which cannot be performed directly (e.g., via an inverse Fourier transformation) because of the unavailability of the full spectrum and phase information. The framework of inverse problems provides a systematic methodology for determining the underlying physical properties of a system by constructing and fine-tuning a mathematical model. Obtaining structural information from scattering data requires solving the inverse problem posed by

$$G(m) = d \tag{1}$$

where $d$ is a set of experimentally observable data and $m$ is the underlying physical model [12]. The operator $G$ performs a transformation which takes a model as input and yields a predicted set of data ($d'$) equivalent to the experimental data $d$. The statement of the inverse problem is to determine the model ($m_s$), via an optimization procedure, such that $||d' - d||$ (where |||| indicates a norm defined on the data space) is minimized. In the case of scattering, $G$ is the Fourier transform of the density profiles associated with the model, $d$ is the set of form factors determined from scattering intensity measurements, and $m$ is a model of the underlying atomic positions. Solving the inverse problem can be complicated by several factors. The solution ($m_s$) may not exist, i.e. the model may be unable to physically represent the data. Conversely, $m_s$ may be an infinite family of acceptable solutions to the problem. This is the case where the number of degrees of freedom of the model exceeds that of the data set. It may also be the case that the problem suffers from instability, i.e. the solution $m_s$ is extremely sensitive to small changes in $d$. Since $d$ often has a noise component, this poses a significant challenge to determining $m_s$. These difficulties can be reduced via regularization procedures which rely on additional physical knowledge of the system (independent of the target data) to reduce the complexity of the problem.

In this paper, we present a new atomic density profile (ADP) model for the determination of lipid bilayer structures. The ADP model, which makes minimal assumptions regarding the atomic arrangement within a lipid molecule, is a significant generalization of the SDP model. The SDP model treats the hydrocarbon core with an error function, and uses a handful of Gaussian functions to describe the head group and backbone. The ADP model treats all atoms (with hydrogens summed into heavy atoms) as independent Gaussian functions. Sophisticated data analysis methodology and fitting procedures are used to systematically assess detailed lipid bilayer structures embedded in SAXS and SANS data. Specifically, an ensemble of optimal ADP models for each lipid bilayer is generated by solving the inverse problem using a simplex based optimization procedure. Ensemble averaging inspired by a Bayesian formulation of the problem yields detailed bilayer structures.

## 2. Model and methods

Models for different lipid bilayer compositions are constructed as follows. Each atom in a lipid molecule, with hydrogens summed into their bonded heavy atoms, is assigned a probability density function. This function represents the distribution of the atom in the one dimensional projection of the bilayer in a leaflet. Since the system is assumed to be homogeneous in the plane of the bilayer, the problem is effectively one dimensional (along bilayer normal). Additionally, the bilayers are assumed to be symmetric with respect to their centers, though the model can be easily extended to asymmetric bilayers. While only pure bilayers are considered, bilayers with arbitrary mixtures of lipids can be treated with the current method. Experimental data ($d$ in Eq. (1)) are SAXS and SANS form factors along with the total lipid molecular volume. Models are regularized using known molecular topology and hydrophobic interactions. A fitness penalty (additional term in $||d' - d||$) for water probability within the hydrocarbon core takes the hydrophobic effect into account. An additional penalty on unphysical probability densities is also employed. Linear constraints on mean atomic positions eliminate models with unphysical bond lengths.

### 2.1. The model (m)

We approximate the probability density of each atom with one normalized Gaussian function of the form:

$$g_i(z) = \frac{1}{\sqrt{2\pi\sigma_i^2}} exp\left[\frac{-(z-\mu_i)^2}{2\sigma_i^2}\right] \tag{2}$$

where $i$ is the index of the atom, $z$ is the distance from bilayer center, and $\mu_i$ and $\sigma_i^2$ are the mean and variance of the distribution respectively.

Both the electron and neutron scattering length densities ($\rho(z)$) for a hydrated lipid bilayer are then calculated by expressing the total density as the sum of lipid, including counter-ions when present ($\rho_{\text{lipid}}(z)$), and water ($\rho_{\text{water}}(z)$) contributions.

$$\rho(z) = \rho_{\text{lipid}}(z) + \rho_{\text{water}}(z) \tag{3}$$

The density profile for the lipid is determined from the probability densities of the atoms ($g_i(z)$).

$$\rho_{\text{lipid}}(z) = \sum_i w_{\alpha_i} \frac{g_i(z)dz}{V_{\text{slice}}} \tag{4}$$

where atom $i$ is of type $\alpha_i$ (e.g., C, O, P or N), $V_{\text{slice}}$ is the volume of a slice of thickness $dz$ along the bilayer normal. The weight on atom $i$ ($w_{\alpha_i}$) is either the number of electrons or the neutron scattering length, depending on the desired density. The contribution from water molecules is written as

$$\rho_{\text{water}}(z) = w_w \frac{p_w(z)dz}{V_{\text{slice}}} \tag{5}$$

where $w_w$ is the corresponding weight for water and $p_w(z)\,dz$ is the number of water molecules between $z$ and $z + dz$, which is unknown. Therefore, from Eq. (3) the density is given by

$$\rho(z) = \sum_i \left[g_i(z;\mu_i,\sigma_i)dz\frac{w_{\alpha_i}}{V_{\text{slice}}}\right] + p_w(z)dz\frac{w_w}{V_{\text{slice}}}. \tag{6}$$

We then set the reference point by subtracting the corresponding density for bulk water:

$$\rho^*(z) = \rho(z) - \rho_{\text{bulk}}(z) \tag{7}$$

$$= \sum_i \left[g_i(z;\mu_i,\sigma_i)dz\frac{w_{\alpha_i}}{V_{\text{slice}}}\right] + (p_w(z)dz - P_w)\frac{w_w}{V_{\text{slice}}} \tag{8}$$

where $P_w$ is the number of water molecules in a slice containing only bulk water. This is given by $P_w = V_{\text{slice}}/v_{\text{bulk}}$ where $v_{\text{bulk}}$ is the partial molecular volume of bulk water. The value for $v_{\text{bulk}}$ was assumed to be 30.0 Å$^3$ based on the density of water at physiologic temperature. Therefore,

$$\rho^*(z) = \sum_i \left[g_i(z;\mu_i,\sigma_i)dz\frac{w_{\alpha_i}}{V_{\text{slice}}}\right] + \left(p_w(z)dz - \frac{V_{\text{slice}}}{v_{\text{bulk}}}\right)\frac{w_w}{V_{\text{slice}}}. \tag{9}$$

The number of water molecules in a slice is chosen, (similar to the SDP model [4]), such that the total molecular volume in a slab equals the slab volume:

$$V_{\text{water}}(z) = V_{\text{slice}} - V_{\text{lipid}}(z) \tag{10}$$

$$V_{\text{water}}(z) = v_w p_w(z)dz \tag{11}$$

$$V_{\text{lipid}}(z) = \sum_i v_{\alpha_i} g_i(z;\mu_i,\sigma_i)dz \tag{12}$$

$$p_w(z)dz = \frac{V_{\text{slice}}}{v_w} - \sum_i \frac{v_{\alpha_i}}{v_w} g_i(z;\mu_i,\sigma_i)dz, \tag{13}$$

where $v_{\alpha_i}$ is the partial volume for species $i$. Substituting Eq. (13) into Eq. (9) we have

$$\rho^*(z) = \sum_i \left[ g_i(z;\mu_i,\sigma_i)dz\left(\frac{w_{\alpha_i}}{V_{\text{slice}}} - \frac{w_w v_{\alpha_i}}{v_w V_{\text{slice}}}\right)\right] + \frac{w_w}{v_w} - \frac{w_w}{v_{\text{bulk}}}. \tag{14}$$

Making the approximation that the molecular volume of interfacial water is similar to that of the bulk, i.e. $v_w \approx v_{\text{bulk}}$, leads to:

$$\rho^*(z) = \frac{dz}{v_w V_{\text{slice}}} \sum_i \left(v_w w_{\alpha_i} - v_{\alpha_i} w_w\right) g_i(z;\mu_i,\sigma_i). \tag{15}$$

Eq. (15) yields $\rho^*(z)$ as the electron or neutron scattering length density, depending on the choice of weights. Weights for each species are given in Table 1. Because of the arbitrary scale of the scattering intensity and the linearity of the cosine transform, the factor of $dz/(v_w V_{\text{slice}})$ is omitted from Eq. (15) during optimization. The densities are computed for one leaflet of the lipid bilayer, then symmetrized to produce even functions. All functions were treated as discrete, with $dz = 0.05$ Å as the granularity for computation of the density functions $\rho^*(z)$.

The set of parameters $\{\mu_i, \sigma_i, v_{\alpha_i}\}$ determines the space for optimization. With three parameters per atom, the dimension of the parameter space is ~160. In order to reduce the size of the parameter space, head group atoms (including counter-ions when present) were assumed to have identical partial volumes. Thus, the set of partial atomic volumes for tuning was $\{v_{\text{CH}_3}, v_{\text{CH}_2}, v_{\text{CH}}, v_{\text{head}}\}$. Additionally, carbon chain atoms of the same type were assumed to have identical $\sigma$ values ($\sigma_{\text{CH}_3}, \sigma_{\text{CH}_2}, \sigma_{\text{CH}}$). Such approximations reduced parameter set sizes from ~160 to ~115.

### 2.2. The data (d)

Different contrast SAXS and SANS form factors for phosphatidylcholine (PC), phosphatidylglycerol (PG), and phosphatidylserine (PS) were obtained from previous works [4–6,8]. Data points which exhibit no discernible scattering signal compared to background noise were truncated. Due to the unavailability of experimental data uncertainties, error bars ($\Delta F_e(q_i)$ in Eq. (17)) were assigned based on the magnitude of scattering signal, as a percentage of the maximum intensity. For the SAXS data, the first lobe is assigned the smallest uncertainty (2%), followed by the second (4%) and third (8%) lobes, while the fourth lobe, when present, is assigned the largest uncertainty (16%). Similar assignments were applied to the SANS data, with two regions defined (4% and 16%). It has been pointed out that the amino $NH_3^+$ group in PS is capable of fast hydrogen–deuterium exchange with the surrounding water [8]. Thus, the $NH_3^+$ hydrogens solvated by water with $x$ mole fraction of $D_2O$ are replaced by $3x$ deuteriums and $3(1-x)$ hydrogens. This has a significant effect on the neutron scattering length profile. Similar exchange also occurs in PG lipids which possess two hydroxyl groups. Although it was not considered in the published PG lipid bilayers using the SDP model [6], the hydrogen–deuterium exchange of PG hydroxyls is taken into account in our ADP model. Lipid volumes, determined using density measurements, were also included in the data sets for optimization. Lipid volumes for parameter tuning were 1303 Å$^3$ for DOPC [4], 1256 Å$^3$ for POPC [5], 1228.5 Å$^3$ for DPPC [4], 1208.7 Å$^3$ for POPG [6], and 1198.5 Å$^3$ for POPS [8].

**Table 1**
Weights for calculation of electron and neutron scattering length densities. Taking hydrogen–deuterium exchange into account, hydroxyl groups in PG and the amine groups in PS were assumed to have hydrogen to deuterium ratios equal to that of the solvent. All other groups are assumed to have neutron scattering cross sections that are not sensitive to $D_2O$ concentration.

| Species | Electron count | Neutron scattering cross-section (fm) | | | |
|---|---|---|---|---|---|
| | | 100% $D_2O$ | 75% $D_2O$ | 70% $D_2O$ | 50% $D_2O$ |
| C | 6 | 6.65 | – | – | – |
| CH | 7 | 2.91 | – | – | – |
| $CH_2$ | 8 | −0.83 | – | – | – |
| $CH_3$ | 9 | −4.57 | – | – | – |
| $N^+$ | 6 | 9.40 | – | – | – |
| $NH_3^+$ | 9 | 29.41 | 21.603 | 20.04 | 13.795 |
| $Na^+$ | 10 | 3.63 | – | – | – |
| P | 15 | 5.17 | – | – | – |
| O | 8 | 5.8 | – | – | – |
| $O^-$ | 9 | 5.8 | – | – | – |
| OH | 9 | 12.47 | 9.868 | 9.347 | 7.265 |
| Water | 10 | 19.24 | 14.035 | 12.994 | 8.83 |

### 2.3. The transformation (G) and the comparison ($||d' - d||$)

To compute the model predicted form factor $F_m(q)$, assuming a symmetric bilayer, the cosine transform was performed.

$$F_m(q) = \int_{-\infty}^{\infty} \rho(z)\cos(qz)dz \tag{16}$$

The degree of agreement between $F_m(q)$ and the experimental form factor ($F_e(q)$) was calculated using

$$\chi = \sqrt{\frac{\sum_{i=1}^{N_q}\left(\frac{k_e F_e(q_i) - F_m(q_i)}{k_e \Delta F_e(q_i)}\right)^2}{N_q - 1}}. \tag{17}$$

where $N_q$ is the number of $q$ values considered and $\Delta F_e(q)$ is the error bar on the experimental value [6]. The $q$-samples for the model generated data were chosen to match the corresponding experimental samples. The experimental form factors must be scaled in order to be comparable with the model data. The factor $k_e$ ensures this appropriate scaling [6].

$$k_e = \frac{\sum_i \frac{F_e(q_i)F_m(q_i)}{[\Delta F_e(q_i)]^2}}{\sum_i \frac{[F_e(q_i)]^2}{[\Delta F_e(q_i)]^2}} \tag{18}$$

The measure of difference ($\chi$) between the model predicted and the experimental form factors was calculated for each set of X-ray data ($\chi_{\text{elec1}}$ and $\chi_{\text{elec2}}$ when two data sets were available) and neutron data ($\chi_{\text{neut100}}$, $\chi_{\text{neut75}}$, $\chi_{\text{neut70}}$, $\chi_{\text{neut50}}$ when sets at 100, 75, 70, and 50% $D_2O$ concentrations were available).

Total lipid molecular volume was included as an additional contribution to the comparison between model and experiment via

$$\chi_{\text{volume}} = \frac{\left|\left(V_{\text{exp}} - \sum_i v_{\alpha_i}\right)\right|}{V_{\text{exp}}}, \tag{19}$$

where $V_{\text{exp}}$ are the experimental volumes.

### 2.4. The regularization

Regularization was introduced in part via linear constraints on the parameter space. Based on molecular dynamics simulation, values for $\sigma_i$ were restricted to the range [2.25, 3.75] Å [13–17]. Partial volumes were constrained as listed in Table 2.

**Table 2**
Constraints on partial atomic volumes. The approximation is that atoms within each group (head, tail CH, tail $CH_2$, and tail $CH_3$) have equal volume.

| Volume | Mini. Value (Å$^3$) | Max. Value (Å$^3$) |
|---|---|---|
| $v_{head}$ | 12.0 | 21.0 |
| $v_{CH}$ | 19.0 | 24.0 |
| $v_{CH_2}$ | 25.0 | 30.0 |
| $v_{CH_3}$ | 51.0 | 56.0 |

Connectivity information was taken into account during optimization by applying relative constraints to all values of $\mu_i$ as follows. Atoms within the *sn*-1 chain were constrained to be within one bond length away from the preceding bonded atom (Eq. (20)), beginning with the terminal methyl group ($i = 0$).

$$\mu_{i-1} \geq \mu_i \geq \mu_{i-1} + b \tag{20}$$

Atoms in the backbone and head group were constrained to be within one bond length of bonded atoms (Eq. (21)).

$$|\mu_i - \mu_k| \leq b \tag{21}$$

Atoms in the *sn*-2 chain were constrained similarly to the *sn*-1 chain (Eq. (22)), but relative to the backbone carbon ($i = 0$).

$$\mu_{i-1} - b \geq \mu_i \geq \mu_{i-1} \tag{22}$$

For optimization the bond length was set to $b = 2.0$ Å. Sodium counter ions were constrained to the range [10, 35]. In order to define a coordinate system, one atom must be chosen as the origin without loss of generality. Since the terminal methyl group of the *sn*-1 chain bilayer can be approximated as bilayer center, the corresponding value for $\mu$ was fixed at $z = 0$. The *sn*-2 terminal methyl group was not similarly restrained. The associated value for $\sigma$ was also variable parameter in the optimization.

Regularization methods were also applied via the addition of penalties on model configurations which have unphysical properties. Models with a probability of finding any lipid atom (including counter-ions) in a slice between $z$ and $z + dz$ ($p_{lipid}(z)$) exceeding unity were penalized by the introduction of the term

$$\chi_{reg1} = \frac{\int_{-\infty}^{\infty} H\{p_{lipid}(z) - 1\}\left[p_{lipid}(z) - 1\right] dz}{\int_{-\infty}^{\infty} H\{p_{lipid}(z) - 1\}}, \tag{23}$$

where $H(x)$ is the Heaviside step function and $p_{lipid}(0) = 1$ defines the reference point. This term (Eq. (23)) penalizes trial models which have regions of negative water probability, which is unphysical. The presence of water in the hydrocarbon core is unfavorable due to hydrophobic

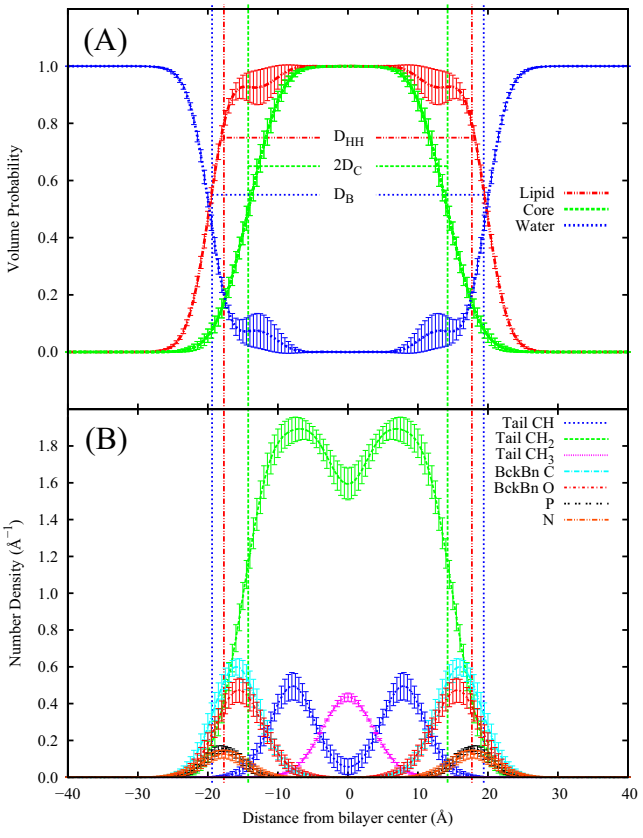


**Fig. 1.** Probability density plots (A) for DOPC included for total lipid, hydrocarbon core, and water. Number densities (B) for hydrocarbon chain groups of the same type (Tail CH, Tail $CH_2$, and Tail $CH_3$), backbone groups (including the carbonyl atoms) of the same type (BckBn O and BckBn C), and head group atoms (P and N). Profiles and structural property locations $D_{HH}$, $2D_C$, $D_B$ are taken from the weighted average of those determined from converged parameter sets. Error bars are determined from the standard deviations of the weighted averages, included only at 0.5 Å intervals for clarity.

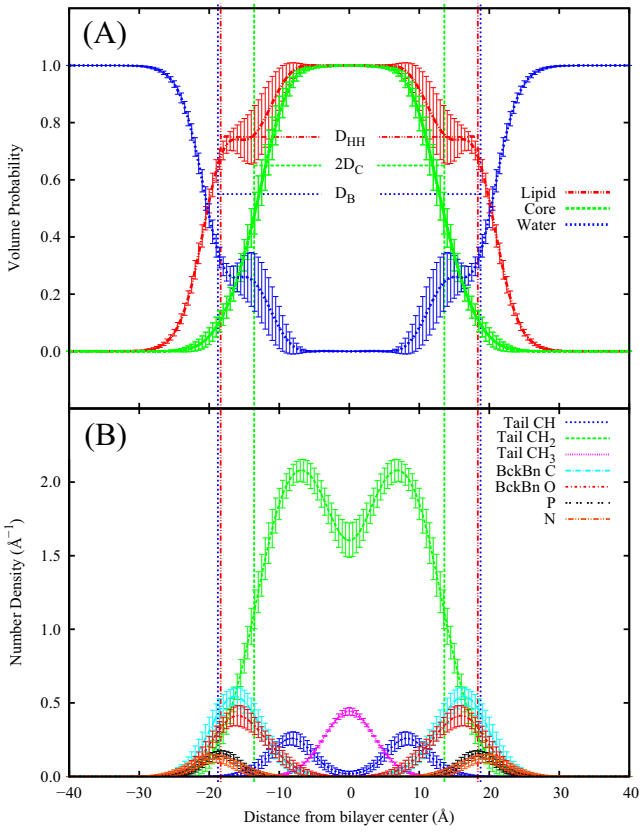


**Fig. 2.** Probability density plots (A) for POPC included for total lipid, hydrocarbon core, and water. Number densities (B) for hydrocarbon chain groups of the same type (Tail CH, Tail $CH_2$, and Tail $CH_3$), backbone groups (including the carbonyl atoms) of the same type (BckBn O and BckBn C), and head group atoms (P and N). Profiles and structural property locations $D_{HH}$, $2D_C$, $D_B$ are taken from the weighted average of those determined from converged parameter sets. Error bars are determined from the standard deviations of the weighted averages, included only at 0.5 Å intervals for clarity.

effects. This physical information is incorporated by introducing the term

$$\chi_{\text{reg2}} = \frac{1}{2\mu_{\text{cut}}}\left[\int_{-\mu_{\text{cut}}}^{\mu_{\text{cut}}} \left(1-p_{\text{lipid}}(z)\right)^2 dz\right]^{1/2} \tag{24}$$

where $\mu_{\text{cut}}$ is defined as the $\mu$ value for the seventh $CH_2$ relative to the carbonyl carbon on the *sn*-1 chain. This regularization term imposes as soft cutoff on the penetration of water into the hydrocarbon core, and is similar in principle to constraints on the hydrocarbon error function parameters in the SDP model [4]. The penalty term in Eq. (24) puts a penalty on water inside of $\mu_{\text{cut}}$, but does not impact water probability above the cutoff. The choice of carbon for $\mu_{\text{cut}}$ is set conservatively, such that small changes in its location have little effect on the optimization results. The cutoff location may need to be adjusted for different lipids and different phases.

### 2.5. Parameter optimization

Optimization of model parameters $\{\mu_i, \sigma_i, v_{\alpha_i}\}$ was performed using the software package ParOpt, a general high dimensional parameter optimization software developed internally [18]. The specific optimization procedure used in this work was Nelder–Mead [19]. Nelder–Mead is designed for optimizing large parameter sets while making very few assumptions regarding the underlying space and target function defined over it. The method is well suited to the specific challenges of this problem, i.e. the large dimensionality (~115) of the space considered and the instability in the calculation of $\|d' - d\|$. An optimization problem for Nelder–Mead is posed by defining both a parameter space and a target function on the space. The parameter space for the current work is the set of parameters $\{\mu_i, \sigma_i, v_{\alpha_i}\}$ bounded by the constraints. The target function for optimization is

$$\mathcal{F}\left(\left\{\mu_i, \sigma_i, v_{\alpha_i}\right\}\right) = \sum_j W_j \chi_j\left(\left\{\mu_i, \sigma_i, v_{\alpha_i}\right\}\right) \tag{25}$$

where $W_j$ are the weight factors for the associated components ($\chi_j$) of the target function and the index $j \in$ {elec1, elec2, neut100, neut75, neut70, neut50, volume, reg1, reg2}. Weights were chosen heuristically to ensure a similar order of magnitude in target function contributions so that all components impact the entire optimization procedure. Weights chosen for optimization were $W_{\text{volume}} = 1000$, $W_{\text{neut}} = 10$, $W_{\text{elec}} = 30$, $W_{\text{reg1}} = 100$, and $W_{\text{reg2}} = 1000$. In the case of DOPC and DPPC, where two sets of experimental X-ray scattering data were included, a value of $W_{\text{elec}} = 15$ was used for each set. A value of $W_{\text{neut}} = 15$ was used for DPPC, since only two $D_2O$ concentrations were available. Nelder–Mead then systematically reduces the value for

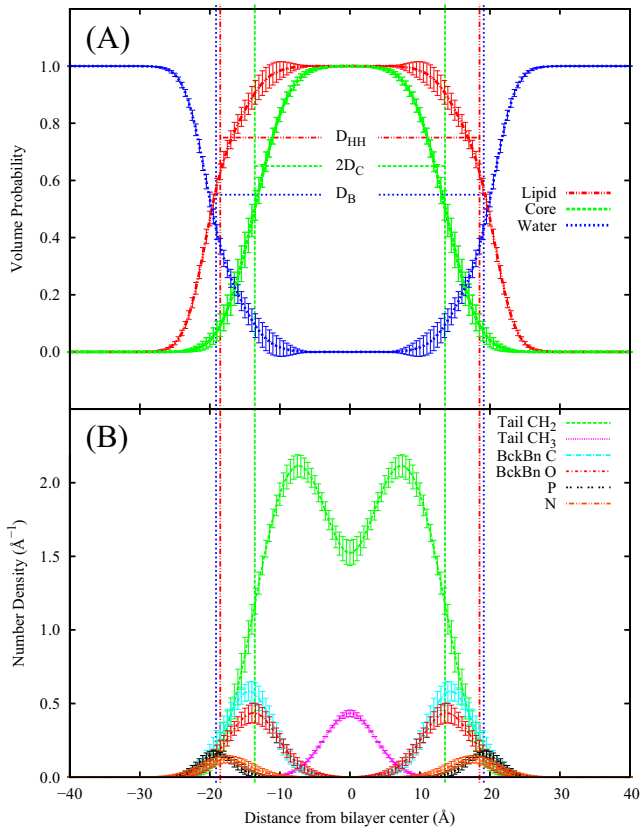


**Fig. 3.** Probability density plots (A) for DPPC included for total lipid, hydrocarbon core, and water. Number densities (B) for hydrocarbon chain groups of the same type (Tail $CH_2$ and Tail $CH_3$), backbone groups (including the carbonyl atoms) of the same type (BckBn O and BckBn C), and head group atoms (P and N). Profiles and structural property locations $D_{HH}$, $2D_C$, $D_B$ are taken from the weighted average of those determined from converged parameter sets. Error bars are determined from the standard deviations of the weighted averages, included only at 0.5 Å intervals for clarity.

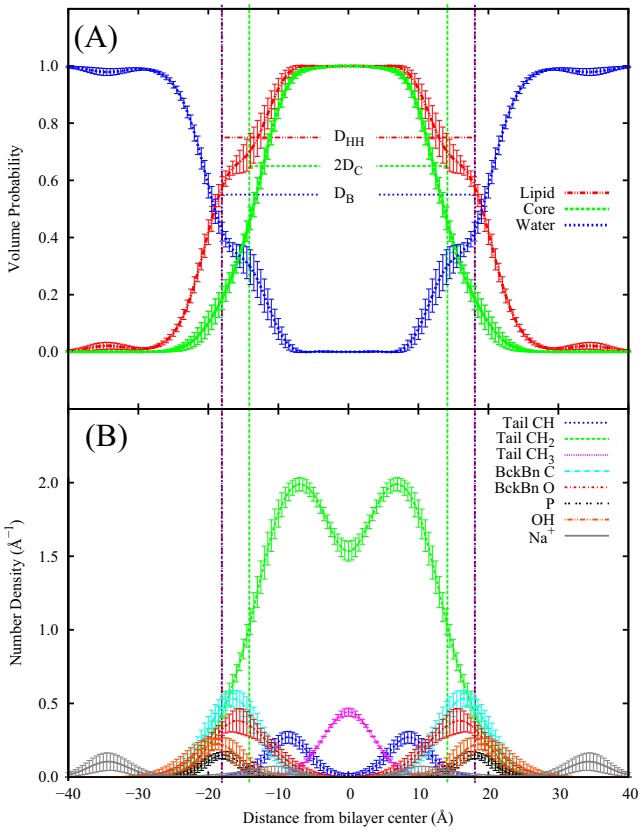


**Fig. 4.** Probability density plots (A) for POPG included for total lipid, hydrocarbon core, and water. Number densities (B) for hydrocarbon chain groups of the same type (Tail CH, Tail $CH_2$, and Tail $CH_3$), backbone groups (including the carbonyl atoms) of the same type (BckBn O and BckBn C), head group atoms (P and OH), and counter ion ($Na^+$). Profiles and structural property locations $D_{HH}$, $2D_C$, $D_B$ are taken from the weighted average of those determined from converged parameter sets. Error bars are determined from the standard deviations of the weighted averages, included only at 0.5 Å intervals for clarity.

$\mathcal{F}\left(\left\{\mu_i, \sigma_i, \nu_{\alpha_i}\right\}\right)$ by evolving a simplex over the parameter space $\left\{\mu_i, \sigma_i, \nu_{\alpha_i}\right\}$. See our previous work for a complete description of the Nelder–Mead algorithm [18]. An optimization of the ADP model to reproduce molecular dynamics simulation data was also performed as an indication of the validity of model assumptions and methods. In the case of MD, both the model *m* and the data *d* are known prior to optimization, allowing the direct comparison of ADP model results and the underlying configuration which generated the data. The ADP model, despite simplifying assumptions, was able to accurately fit the low noise, high angle range MD data. The procedure and results for comparison with MD are described in detail in the Appendix A.

## 3. Results

A consequence of the atomistic nature of the ADP model is that the number of effectively independent data points is smaller than the number of free parameters in the model, despite the regularization procedure described above. This issue can be only resolved with either further regularization or inclusion of more observations (e.g., neutron scattering of selectively deuterated lipids [3,4]). More regularization is not feasible due to the lack of additional physical information. Thus, there are many points in the parameter space (i.e. models for the bilayer configuration) that match the data equivalently well within the margins of experimental error. In other words, the condition of uniqueness is not met, and we expect to see multiple minima in the target function $\mathcal{F}$ in Eq. (25). Each instance of parameter set optimization by the Nelder–Mead method began with random initial configurations. Since the optimization is underdetermined, the converged value depends on the initial configuration, leading to many different optimal models. Since these different models represent the data similarly well, they must all be considered as plausible physical configurations for the bilayer. We therefore consider many such models (200 converged points for each lipid), and employ a weighted averaging procedure to obtain structural information, as outlined below.

The weighted average of quantity *A* is

$$\bar{A} = \frac{\sum_k \omega_k A_k}{\sum_k \omega_k} \tag{26}$$

where for the *k*th optimal model, $\omega_k$ is the (non-negative) weight and $A_k$ is the value of *A*. A measure of variability of $\bar{A}$ is

$$\sigma = \sqrt{\frac{\sum_k \omega_k \left(A_k - \bar{A}\right)^2}{\sum_k \omega_k}}. \tag{27}$$

In order to assign greater importance to models that match the data more closely, for the *k*th optimal model with target function value $\mathcal{F}_k$, weights ($\omega_k$) are chosen to be proportional to $exp(-\mathcal{F}_k)$. To ensure numerical stability, we therefore define

$$\omega_k = exp[-(\mathcal{F}_k - \mathcal{F}_1)] \tag{28}$$

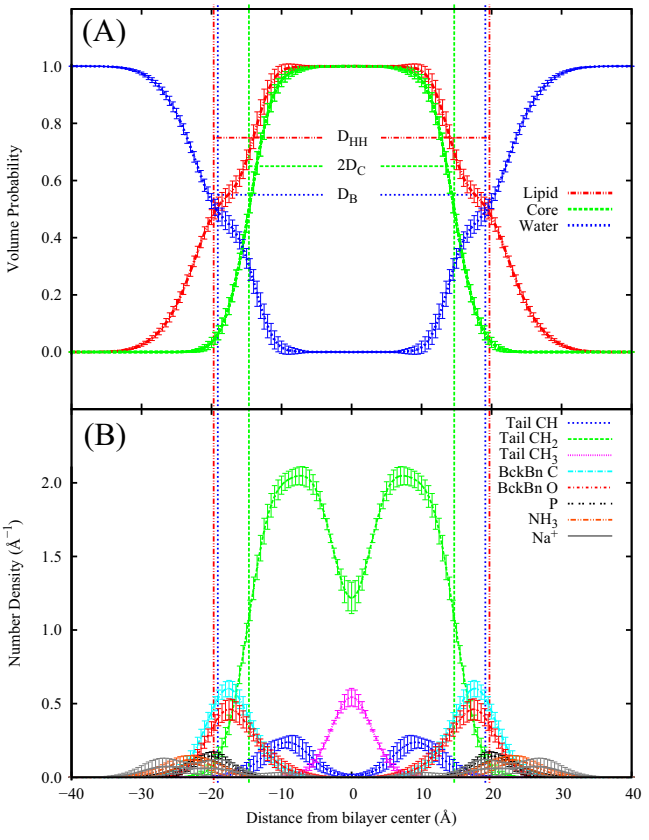


**Fig. 5.** Probability density plots (A) for POPS included for total lipid, hydrocarbon core, and water. Number densities (B) for hydrocarbon chain groups of the same type (Tail CH, Tail $CH_2$, and Tail $CH_3$), backbone groups (including the carbonyl atoms) of the same type (BckBn O and BckBn C), head group atoms (P and $NH_3$), and counter ion ($Na^+$). Profiles and structural property locations $D_{HH}$, $2D_C$, $D_B$ are taken from the weighted average of those determined from converged parameter sets. Error bars are determined from the standard deviations of the weighted averages, included only at 0.5 Å intervals for clarity.

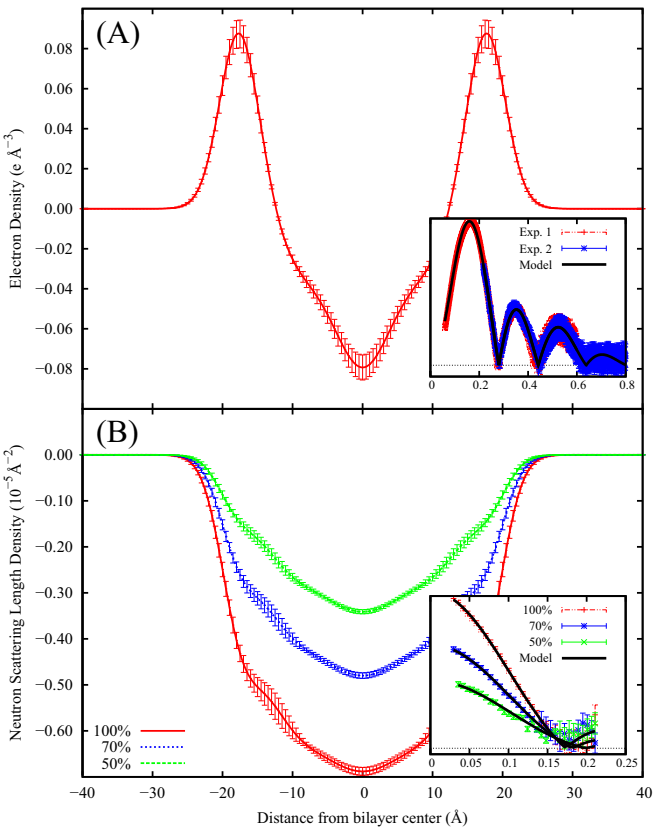


**Fig. 6.** Electron (A) and neutron scattering length (B) densities, relative to bulk water, shown for DOPC. Example fits of the lowest target function value point, with model and measured form factors (arbitrary units) as a function of scatting vector q (Å$^{-1}$), are included as insets. Percentages indicate $D_2O$ concentration.

where $\mathcal{F}_1$ is the lowest value for the target function over the set of optimal models considered for averaging.

The exponential form of the weights $\omega_k$ in Eq. (28) is motivated by analogy with a Bayesian [20] statistical formulation of the problem. Though our target function has the form $\mathcal{F} = \chi + $ physically − based regularization terms (Eq. (25)), a strict Bayesian formulation of the same problem under the assumption of Gaussian noise with known variance structure would lead to a target function of the form $\mathcal{F}' = \chi^2 +$ physically − based regularization terms. In such a Bayesian formulation, the regularization terms together represent the negative logarithm of the prior distribution, and $\chi^2$ is the negative logarithm of the likelihood function. The posterior distribution, which is the prime inferential object of the Bayesian machinery, has the form $exp(-\mathcal{F}')$. Further, it is a probability (density) function that weighs all possible bilayer models with respect to the data and the prior information. Therefore, it provides weight according to the relative fitness of model. A superficially similar exponential form for averaging weights can also be found in the context of multimodel inference based on information criteria such as Akaike or Bayesian information criteria (BIC) [21]. The use of $\mathcal{F}$ instead of $\mathcal{F}'$ is motivated by historical precedent. The usage of $\chi$ has been preferred in previous works, especially in applications of the SDP model [4–8]. A rigorous statistical formulation, Bayesian or otherwise, would require careful modeling of the noise in the data. In practice, given the uncertainties in the data [22,23], we do not expect serious discrepancy in the predictions based on $\mathcal{F}$ and $\mathcal{F}'$.

### 3.1. Structural properties

Subfigure (A) of Figs. 1 to 5 shows volume probabilities for the hydrocarbon core, total lipid, and water. Average structural characteristics peak-to-peak distance ($D_{HH}$), overall bilayer thickness ($D_B$), and hydrocarbon core thickness ($D_C$) are also indicated. Regions of increased uncertainty in the water and lipid density profiles are found within the head group region for all lipids. The magnitude of this increase in uncertainty depends on the lipid, being most extreme in DOPC (Fig. 1) and POPC (Fig. 2). These regions indicate the possible presence of a hydration layer within the backbone region, in contrast to a smooth drop from interfacial to bulk water. Areas of water concentration within the head group have been proposed by both theory [24] and experiment [25]. The counter ion distribution for the two acidic lipids (POPG and POPS) differs substantially. The sodium ion in POPS is more strongly associated with the head group than that of POPG. Subfigure (B) of Figs. 1 to 5 shows the number density for different subgroups within a lipid molecule. Tail groups include atoms from both hydrocarbon chains of the same type (Tail CH, Tail $CH_2$, and Tail $CH_3$). The groups BckBn C and BckBn O include atoms of the respective type in both the glycerol backbone and carbonyl groups.

Figs. 6 to 10 show weighted averages of the electron and neutron scattering length densities for each lipid. Insets contain example fits chosen from the converged point with the lowest value for the target function ($\mathcal{F}_1$), along with experimental data and the experimental error bars.

Table 3 lists the weighted averages of several important structural properties for lipid bilayers composed of DOPC, POPC, DPPC, POPG, and POPS determined using the ADP model. In general, our ADP model gives rise to lipid bilayer structures that are consistent with those obtained from the SDP model [4–8]. The partial component volumes ($V_{head}$, $V_{core}$, $v_{CH}$, $v_{CH_2}$, and $v_{CH_3}$) are similar to those reported by the SDP model. Peak-to-peak distance ($D_{HH}$) is defined as twice the distance from the bilayer center to the maximum value in the electron

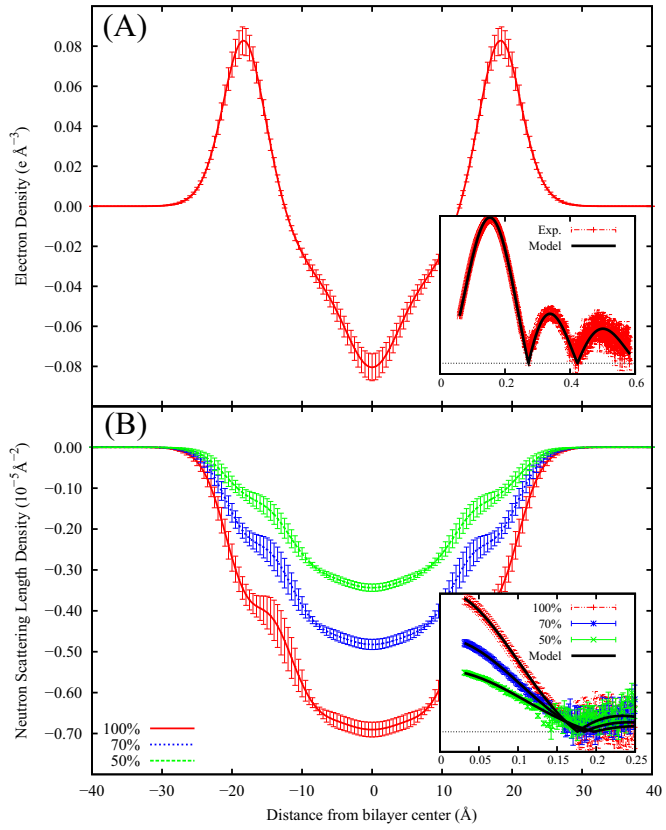


**Fig. 7.** Electron (A) and neutron scattering length (B) densities, relative to bulk water, shown for POPC. Example fits of the lowest target function value point, with model and measured form factors (arbitrary units) as a function of scatting vector q (Å$^{-1}$), are included as insets. Percentages indicate $D_2O$ concentration.

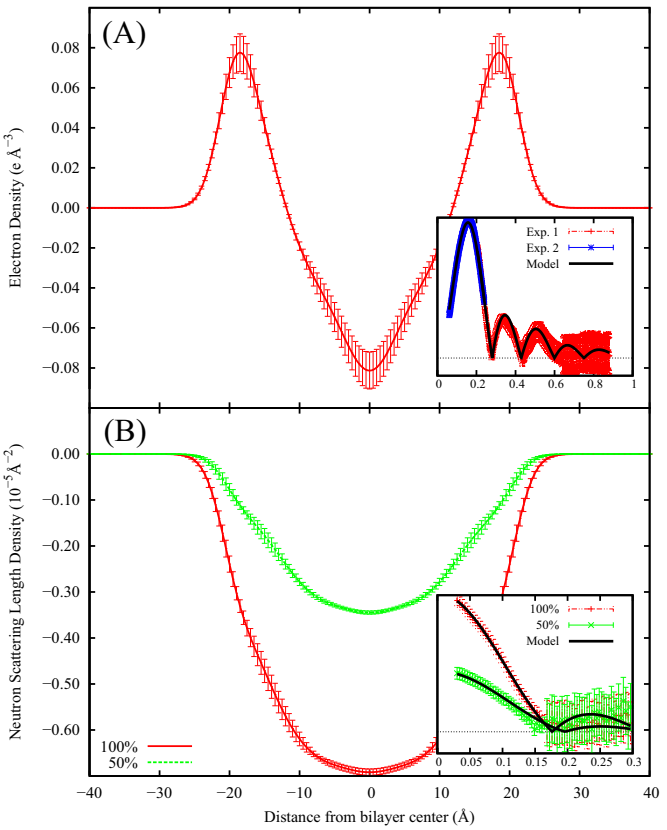


**Fig. 8.** Electron (A) and neutron scattering length (B) densities, relative to bulk water, shown for DPPC. Example fits of the lowest target function value point, with model and measured form factors (arbitrary units) as a function of scatting vector q (Å$^{-1}$), are included as insets. Percentages indicate $D_2O$ concentration.

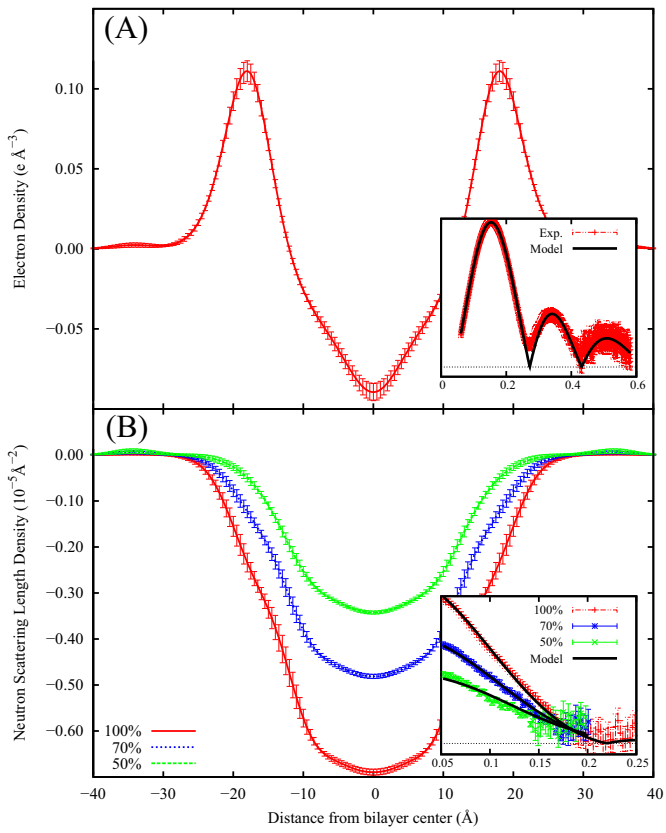


**Fig. 9.** Electron (A) and neutron scattering length (B) densities, relative to bulk water, shown for POPG. Example fits of the lowest target function value point, with model and measured form factors (arbitrary units) as a function of scatting vector q (Å$^{-1}$), are included as insets. Percentages indicate $D_2O$ concentration.

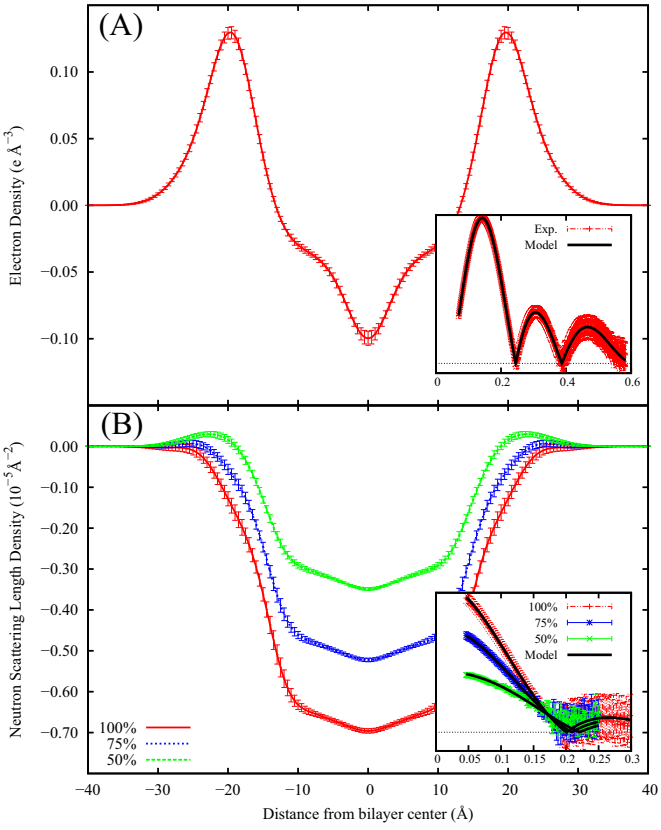


**Fig. 10.** Electron (A) and neutron scattering length (B) densities, relative to bulk water, shown for POPS. Example fits of the lowest target function value point, with model and measured form factors (arbitrary units) as a function of scatting vector q (Å$^{-1}$), are included as insets. Percentages indicate $D_2O$ concentration.

density profile. Overall bilayer thickness ($D_B$) was calculated by solving the following equation for $D_B$ [26,27]:

$$\int_0^{D_B/2} \left(1-p_{\text{lipid}}(z)\right)dz = \int_{D_B/2}^{\infty} p_{\text{lipid}}(z)dz. \tag{29}$$

The thickness of the hydrocarbon core, excluding the chain carbonyl groups, ($2D_C$) was similarly determined by solving:

$$\int_0^{D_C} (1-p_{\text{core}}(z))dz = \int_{D_C}^{\infty} p_{\text{core}}(z)dz. \tag{30}$$

See Fig. 11 for an illustration of the $D_B$ and $2D_C$ calculations. The overall bilayer thickness $D_B$ and hydrocarbon chain thickness $2D_C$ obtained from our ADP model conform to those reported by SDP model [4–8]. Area per lipid ($A$) which reflects the lipid bilayer lateral packing property, was calculated from

$$A = \frac{V_{\text{lipid}}}{D_B/2}. \tag{31}$$

Results for area are also consistent with those of the SDP model which has a lipid area uncertainty of 1–2 Å$^2$ [4]. For the three PC lipids, our ADP model predicts 63.8, 67.0 and 67.2 Å$^2$ for DPPC, POPC and DOPC, respectively, while the corresponding lipid areas based on SDP model are 63.1, 64.3, and 67.4 Å$^2$ [4,5]. The lipid area of POPG determined using our ADP model is 66.9 Å$^2$. This value is in good agreement with the reported 66.1 Å$^2$ using SDP model which did not model hydrogen–deuterium exchange [6]. For the apoptosis related POPS lipid, our ADP model yields a lipid area of 62.7 Å$^2$, which is in also in excellent agreement with the value 62.7 Å$^2$ reported using the SDP model [8].

For the DPPC bilayer, unlike other lipids, the sum of lipid component volumes $V_{\text{head}}$ and $V_{\text{core}}$ is not equal to the target value for total lipid volume ($V_{\text{exp}}$). The model structures which best fit the scattering data are consistent with a total lipid volume of 1219.5 ± 2.4 Å$^3$ which is substantially lower than the target value of 1228.5 Å$^3$. Since the precision of the total volume is higher than the difference between the target and model predicted values, this discrepancy is an important result of the fitting.

Despite the similar structural parameters resulting from the ADP and SDP models, the method and model presented in this work offers several advantages: (1) the ADP model yields atomic distributions, while only group information can be obtained from the SDP model, (2) the ADP model requires minimal constraints on parameters aside from regularization considerations such as physical bond length, while the SDP model demands many more soft constrained parameters in order to obtain stable fitting (e.g., the error function width), (3) variance in model prediction indicates the precision with which scattering data can predict structural properties, and (4) the ADP model can be easily extended to complicated systems such as lipid mixtures and transmembrane proteins.

## 4. Conclusion

We have developed a general method using the ADP model for the determination of lipid membrane structures via SAXS and SANS data. The method relies on an in-house software package ParOpt which is available for download under the GNU public license at https://

**Table 3**
Lipid structural properties determined from model averages. Hydrogen–deuterium exchange is taken into account for hydroxyl groups in POPG and the amine group in POPS. Values shown are weighted averages using Eq. (26) and standard deviations using Eq. (27) of 200 optimized models. Weights were determined using Eq. (28). Head includes head group, glycerol backbone, and the carbonyl groups. Core group fatty acid tails, excluding the carbonyl groups.

| | DOPC | POPC | DPPC | POPG | POPS |
|---|---|---|---|---|---|
| $V_{head}(Å^3)$ | 346.7 ± 16.4 | 346.7 ± 17.8 | 353.3 ± 24.7 | 263.0 ± 15.6 | 278.7 ± 9.1 |
| $V_{core}(Å^3)$ | 956.3 ± 16.4 | 909.3 ± 17.8 | 866.2 ± 26.9 | 945.7 ± 15.6 | 919.8 ± 9.1 |
| $v_{CH}(Å^3)$ | 22.6 ± 1.3 | 22.1 ± 1.7 | – | 21.9 ± 1.8 | 21.4 ± 1.9 |
| $v_{CH_2}(Å^3)$ | 27.2 ± 0.7 | 27.2 ± 0.6 | 27.2 ± 0.9 | 28.5 ± 0.5 | 27.5 ± 0.4 |
| $v_{CH_3}(Å^3)$ | 51.9 ± 1.1 | 52.2 ± 1.4 | 51.9 ± 1.1 | 52.4 ± 1.5 | 54.2 ± 1.5 |
| $D_{HH}(Å)$ | 35.4 ± 0.1 | 36.7 ± 0.2 | 37.0 ± 0.2 | 36.1 ± 0.3 | 39.4 ± 0.3 |
| $D_B(Å)$ | 38.8 ± 0.5 | 37.5 ± 1.0 | 38.2 ± 0.4 | 36.2 ± 0.4 | 38.2 ± 0.3 |
| $2D_C(Å)$ | 28.5 ± 0.6 | 27.2 ± 1.0 | 27.2 ± 0.7 | 28.3 ± 0.5 | 29.3 ± 0.3 |
| $A(Å^2)$ | 67.2 ± 0.9 | 67.0 ± 1.8 | 63.8 ± 0.7 | 66.9 ± 0.7 | 62.7 ± 0.5 |

csmlabfs1.cas.usf.edu/Sites [18]. The method optimizes the ADP model which makes minimal assumptions on the underlying atomic structure. The paucity of experimental data and the overabundance of free parameters are overcome by applying regularization methods, i.e. parameters are constrained to reflect molecular topology and penalty terms are added to take hydrophobic interactions into account. Despite these reductions in redundancy, the model remains underdetermined. Since all solutions to the problem are equally valid, structure predictions from all optimal models are averaged, using a weight factor inspired by Bayesian information criterion. This allows us to present bilayer structures using atomic models, a level of detail that was not achievable in previously published methods. The greater flexibility of the ADP model and the more rigorous fitting procedure described above has yielded bilayer structure comparable to existing work. The increased level of detail in the ADP model produces bilayer structures with the possibility of a distinct hydration layer within the interfacial region. In future work, the ADP model will be applied to lipid bilayer systems that are too complex for simpler models.

## Acknowledgements

The authors thank Prof. John Nagle and Prof. John Katsaras for valuable notes on this manuscript. Authors JCF and SAP would like to thank NIH for partial support at various stages of this work under grant 1R01GM086707-01A1.

## Appendix A

As a test case of the ADP model and the optimization methods presented here, we performed similar analysis with lipid bilayer form factors determined from molecular dynamics (MD) simulation as the target. In the case of MD, unlike with experimental data, we can compare our solutions of the inverse problem (Eq. (1)) with the actual model ($m$) which gave rise to the data $d$. Therefore, tuning the ADP model to reproduce MD data provides a test of the reproducibility of $G$ given $m$ and $d$.

Molecular dynamics simulations were performed on a system consisting of 128 POPC molecules and 100 water molecules per lipid using GROMACS version 4.0 [28]. The system was run under a constant temperature and pressure ensemble with a temperature of 303 K and a pressure of 1 bar for 200 ns with timestep of 2 fs. Long-range electrostatic interactions (beyond 0.95 nm) were computed using the Particle Mesh Ewald method. Lennard–Jones interactions were computed for all distances up to 1.8 nm. Interaction parameters were used from ffG43A1-S3 [29]. Time averaged electron and neutron scattering length

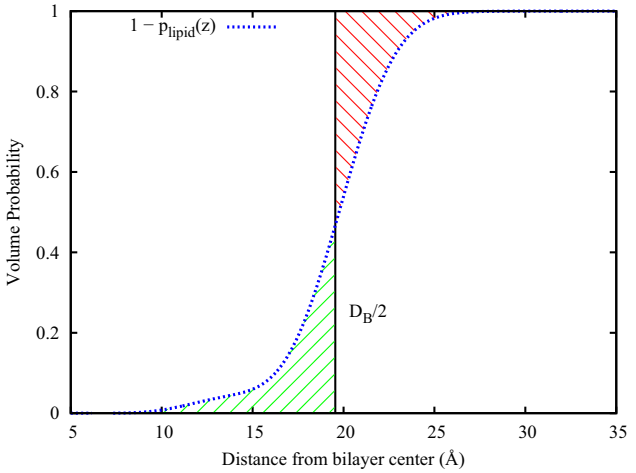


**Fig. 11.** Calculation of $D_B$ for DOPC. A similar calculation is performed to calculate $2D_C$ with the hydrocarbon core atom probability. The location of $D_B/2$ is the Gibbs dividing surface, where the two shaded areas are equal.

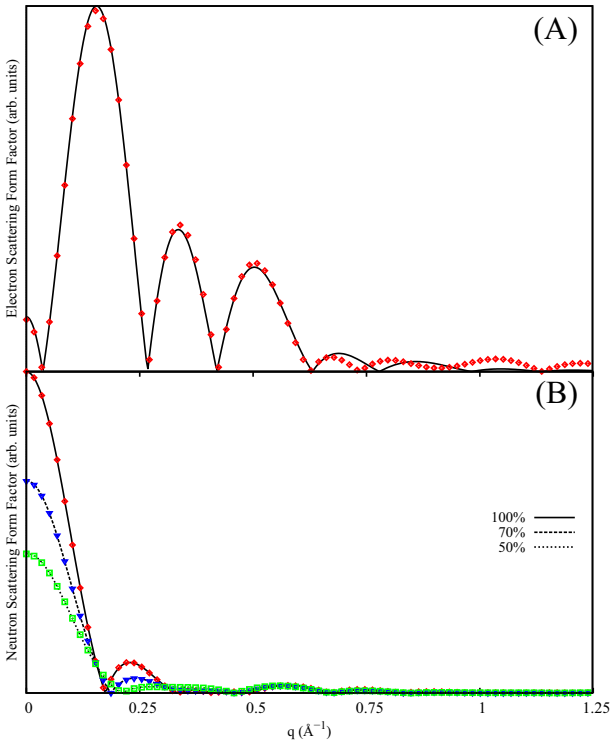


**Fig. 12.** Electron (A) and neutron (B) scattering form factors determined from molecular dynamics simulation (points) and optimization of the ADP model (lines) with the MD form factors as targets.

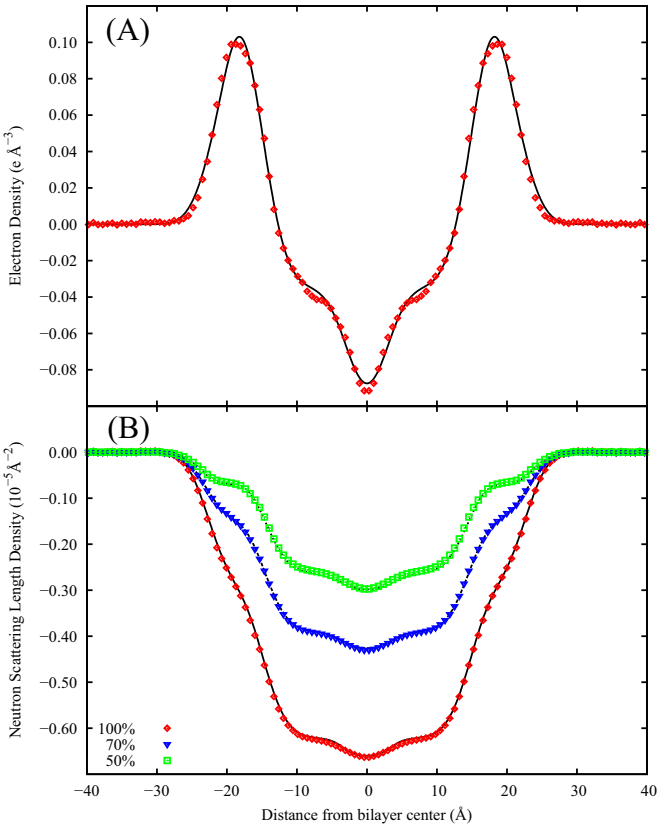


**Fig. 13.** Electron (A) and neutron scattering length (B) relative to bulk water densities for MD (points) and the ADP model fit (lines). Since a constant scalar multiple has been removed during calculation of form factors, the ADP results are re-scaled.

densities were extracted from the final 10 ns of the simulation trajectory using the GROMACS included analysis utilities. A cosine transformation (Eq. (16)) was performed to generate scattering form factors. Though only $H_2O$ was used in the simulations, neutron scattering lengths corresponding to solvent $D_2O$ concentrations of 100%, 70% and 50% were used in order to generate data similar to the experimental case.

These form factors determined from MD simulation, along with the experimental value for total lipid volume, and regularization terms

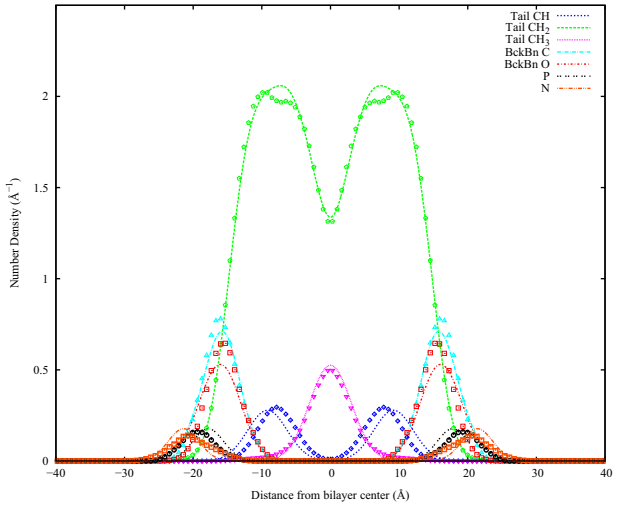


**Fig. 14.** Number densities for groups of atoms determined from MD simulation (points) compared with the fitted ADP model (lines).

$\chi_{reg1}$ (Eq. (23)) and $\chi_{reg1}$ (Eq. (24))) were used to optimize the ADP model. Fig. 12, which shows optimized ADP model form factors compared with the target MD form factors for one optimization. The ADP model is able to very accurately reproduce the scattering form factors even for large values of $q$ despite all the simplifying assumptions. We conclude that the ADP model and our optimization technique are best suited to fit the scattering data and extract the structural properties. If the target data are generated with low error and high q values the model reproduction is near perfect (see Figs. 12 and 13). For real experimental systems where high errors are inevitable and the range of $q$ is truncated due to instrumental limitations, we used sophisticated statistical methods to choose the model. Fig. 13 compares the optimized ADP model real space structure (lines) with the molecular dynamics analysis (points). The important structural characteristics of the lipid bilayer are recovered from the MD data by the ADP model, despite several simplifying assumptions. Differences in real space density scale between the MD and ADP results can result from difference in total lipid volume differences between MD and the experimental value used for ADP optimization and the insensitivity of the transformations to scale. Fig. 14 shows the number densities of selected groups of atom types for MD (points) and ADP (lines). The ADP model and optimization have recovered the main features of atomic distributions.

## References

[1] Richard C. Aster, Brian Borchers, Clifford H. Thurber, Parameter Estimation and Inverse Problems, Elsevier, San Diego, 2004.
[2] O. Berger, O. Edholm, F. Jähnig, Molecular dynamics simulations of a fluid bilayer of dipalmitoylphosphatidylcholine at full hydration, constant pressure, and constant temperature, Biophys. J. 72 (5) (1997) 2002–2013.
[3] K.P. Burnham, D.R. Anderson, Model Selection and Multimodel Inference, Springer, New York, 2002.
[4] See-Wing Chiu, Sagar A. Pandit, H.L. Scott, Eric Jakobsson, An improved united atom force field for simulation of mixed lipid bilayers, J. Phys. Chem. B 113 (9) (2009) 2748–2763 (PMID: 19708111).
[5] Jhuma Das, Elijah Flenner, Ioan Kosztin, Anomalous diffusion of water molecules in hydrated lipid bilayers, J. Chem. Phys. 139 (6) (2013) 065102.
[6] Joseph C. Fogarty, See-Wing Chiu, Peter Kirby, Eric Jakobsson, Sagar A. Pandit, Automated optimization of water–water interaction parameters for a coarse-grained model, J. Phys. Chem. B 118 (6) (2014) 1603–1611.
[7] N.P. Franks, W.R. Lieb, The structure of lipid bilayers and the effects of general anaesthetics: an x-ray and neutron diffraction study, J. Mol. Biol. 133 (4) (1979) 469–500.
[8] Andrew Gelman, John B. Carlin, Hal S. Stern, David B. Dunson, Aki Vehtari, Donald B. Rubin, Bayesian Data Analysis, third edition Chapman and Hall/CRC, 2013.
[9] Peter Heftberger, Benjamin Kollmitzer, Frederick A. Heberle, Jianjun Pan, Michael Rappolt, Heinz Amenitsch, Norbert Kučerka, John Katsaras, Georg Pabst, Global small-angle x-ray scattering data analysis for multilamellar vesicles: the evolution of the scattering density profile model, J. Appl. Crystallogr. 47 (1) (Feb 2014) 173–180.
[10] Berk Hess, Carsten Kutzner, David van der Spoel, Erik Lindahl, Gromacs 4: algorithms for highly efficient, load-balanced, and scalable molecular simulation, J. Chem. Theory Comput. 4 (3) (2008) 435–447.
[11] Jeffery B. Klauda, Norbert Kucerka, Bernard R. Brooks, Richard W. Pastor, John F. Nagle, Simulation-based methods for interpreting x-ray data from lipid bilayers, Biophys. J. 90 (8) (Apr 2006) 2796–2807.
[12] Jeffery B. Klauda, Richard M. Venable, J. Alfredo Freites, Joseph W. O'Connor, Douglas J. Tobias, Carlos Mondragon-Ramirez, Igor Vorobyov, Alexander D. MacKerell, Richard W. Pastor, Update of the CHARMM all-atom additive force field for lipids: validation on six lipid types, J. Phys. Chem. B 114 (23) (2010) 7830–7843.
[13] Norbert Kučerka, Bryan W. Holland, Chris G. Gray, Bruno Tomberli, John Katsaras, Scattering density profile model of POPG bilayers as determined by molecular dynamics simulations and small-angle neutron and x-ray scattering experiments, J. Phys. Chem. B 116 (1) (2012) 232–239.
[14] Norbert Kučerka, John F. Nagle, Jonathan N. Sachs, Scott E. Feller, Jeremy Pencer, Andrew Jackson, John Katsaras, Lipid bilayer structure determined by the simultaneous analysis of neutron and x-ray scattering data, Biophys. J. 95 (5) (2008) 2356–2367.
[15] Norbert Kučerka, Mu-Ping Nieh, John Katsaras, Fluid phase lipid areas and bilayer thicknesses of commonly used phosphatidylcholines as a function of temperature, Biochim. Biophys. Acta Biomembr. 1808 (11) (2011) 2761–2771.
[16] Jahur A. Mondal, Satoshi Nihonyanagi, Shoichi Yamaguchi, Tahei Tahara, Three distinct water structures at a zwitterionic lipid/water interface revealed by heterodyne-detected vibrational sum frequency generation, J. Am. Chem. Soc. 134 (18) (2012) 7842–7850.
[17] J.F. Nagle, S. Tristram-Nagle, Structure of lipid bilayers, Biochim. Biophys. Acta 1469 (3) (Nov 2000) 159–195.
[18] J.A. Nelder, R. Mead, A simplex method for function minimization, Comput. J. 7 (4) (1965) 308–313.

[19] J. Nocedal, S. Wright, Numerical optimization, Springer Series in Operations Research and Financial Engineering, Springer, 2006.
[20] Sagar A. Pandit, See-Wing Chiu, Eric Jakobsson, Ananth Grama, H.L. Scott, Cholesterol packing around lipids with saturated and unsaturated chains: a simulation study, Langmuir 24 (13) (2008) 6858–6865.
[21] Jianjun Pan, Xiaolin Cheng, Luca Monticelli, Frederick A. Heberle, Norbert Kucerka, D. Peter Tieleman, John Katsaras, The molecular structure of a phosphatidylserine bilayer determined by scattering and molecular dynamics simulations, Soft Matter 10 (2014) 3716–3725.
[22] Jianjun Pan, Frederick A. Heberle, Stephanie Tristram-Nagle, Michelle Szymanski, Mary Koepfinger, John Katsaras, Norbert Kučerka, Molecular structures of fluid phase phosphatidylglycerol bilayers as determined by small angle neutron and x-ray scattering, Biochim. Biophys. Acta Biomembr. 1818 (9) (2012) 2135–2148.
[23] V.A. Parsegian, R.P. Rand, Interaction in membrane assemblies, in: R. Lipowsky, E. Sackmann (Eds.), Structure and Dynamics of Membranes, Volume 1 of Handbook of Biological PhysicsNorth-Holland, 1995, pp. 643–690.
[24] Brian Richard Pauw, Everything SAXS: small-angle scattering pattern collection and correction, J. Phys. Condens. Matter 25 (38) (2013) 383201.
[25] B.R. Pauw, Corrigendum: everything SAXS: small-angle scattering pattern collection and correction (2013 J. Phys.: Condens. Matter 25 383201), J. Phys. Condens. Matter 26 (23) (2014) 239501.
[26] Nam Dinh Pham, Bogdan M. Wilamowski, Improved Nelder Mead's simplex method and applications, J. Comput. 3 (3) (2011).
[27] K. Tu, D.J. Tobias, M.L. Klein, Constant pressure and temperature molecular dynamics simulation of a fully hydrated liquid crystal phase dipalmitoylphosphatidylcholine bilayer, Biophys. J. 69 (6) (1995) 2558–2562.
[28] M.C. Wiener, S.H. White, Fluid bilayer structure determination by the combined use of x-ray and neutron diffraction. I. Fluid bilayer models and the limits of resolution, Biophys. J. 59 (1) (1991) 162–173.
[29] M.C. Wiener, S.H. White, Structure of a fluid dioleoylphosphatidylcholine bilayer determined by joint refinement of x-ray and neutron diffraction data. III. Complete structure, Biophys. J. 61 (2) (1992) 434–447.